Desalination and Water Treatment
www.deswater.com
doi: 10.5004/dwt.2020.25640

189 (2020) 357–366
June

Novel iron manganese oxide modified mulberry biochar for the adsorption of phosphorus in aqueous solution

Meina Liang[a,b], Liling Yan[a], Dunqiu Wang[a,b,*], Xu Cheng[a], Zhenliang Deng[a], Shuiping Xu[a], Sen Li[a]

[a]*College of Environmental Science and Engineering, Guilin University of Technology, Guilin 541004, China, Tel. +86-137-0783-7606; email: wangdunqiu@sohu.com (D. Wang), Tel. +86-150-7836-7985; email: liangmeinaa@163.com (M. Liang), Tel. +86-131-9773-8710; email: 578015748@qq.com (L. Yan), Tel. +86-158-2010-6476; email: 707062937@qq.com (X. Cheng), Tel. +86-152-7732-5579; email: dengzhenliang088@163.com (Z. Deng), Tel. +86-159-7738-8910; email: 641282431@qq.com (S. Xu), Tel. +86-186-7737-8987; email: 215326776@qq.com (S. Li)*
[b]*Guangxi Key Laboratory of Environmental Pollution Control Theory and Technology, Guilin 541004, China*

Received 10 August 2019; Accepted 3 February 2020

ABSTRACT

The modified iron manganese oxide modified mulberry biochar (IMOM-BC) sorbent was prepared by chemical oxidation and coprecipitation. Scanning electron microscope, Fourier-transform infrared spectroscopy, X-ray diffraction, and X-ray photoelectron spectroscopy were employed to analyze the adsorption mechanism of IMOM-BC for phosphorus. The effects brought by different pH values, adsorbent dosages, contact time, and coexisting ions on the adsorption were investigated. The results show that IMOM-BC with pH 2.0 can adsorb phosphorus best, and with a dosage of 2.0 g/L, the removal rate of phosphorus can reach 99.85%. Here the adsorption effect for coexisting ions of phosphorus is $CO_3^{2-} > SO_4^{2-} > NO_3^-$. The Langmuir isotherm adsorption model can be referred to explain the adsorption process of phosphorus by IMOM-BC. At 25°C, 35°C, and 45°C, the maximum adsorption capacity for phosphorus were 23.09, 25.32, and 26.34 mg/g, respectively. The iron, manganese oxide, surface hydroxyl, and phenolic hydroxyl groups of IMOM-BC are found to be involved in the adsorption, and the adsorption of phosphorus by IMOM-BC is considered to be mainly chemical adsorption.

Keywords: Mulberry; Adsorption; Phosphorus; Biochar

1. Introduction

Phosphorus is an essential nutrient in the water environment, but excessive phosphorus in the water causes eutrophication in the reservoirs, lakes, and coastal areas [1,2]. Eutrophication is a global environmental issue. The phosphorus in water mainly comes from industrial wastewater, domestic sewage, and farmland drainage. The removal methods of phosphorus-containing wastewater primarily include chemical methods, biological methods, and physical methods [3]. Metal oxides such as iron and manganese are reported to be used in the adsorption and removal of arsenic, volatile organic compounds, and heavy metals [4,5] in water. Iron oxide is superior in adsorbing arsenic and phosphorus, and is simple to prepare and environmentally friendly [6]. In addition, manganese oxide shows a better affinity for heavy metals than iron oxide, which provides an effective route for removing many heavy metals [7]. To overcome disadvantages of lower specific surface area and easy agglomeration of pure iron-manganese oxides, metal oxides are often loaded onto inexpensive

* Corresponding author.

dielectric materials using simple methods [8–10]. Therefore, the loading of metal oxides is beneficial to increase the positive charge on the surface of the modified biochar, and facilitate the adsorption of negative electron elements such as phosphorus [11]. Through loaded or modified metal oxide materials onto inexpensive dielectric materials, the effective specific surface area of the obtained material increases, making them promising functional materials for the removal of contaminant from water.

As a major sericulture province, Guangxi produced 378,000 tons of cocoon in 2016, whereas in 2017, it increased by 4.8% [12]. While bringing economic benefits, a large number of discarded mulberry rods demand an effective exploitation urgently and thus need immediate attention. Phosphate is a typical contaminant in the waste water. The current study was aimed to prepare a novel cost-effective biochar sorbent for phosphate removal. To reduce the cost of biochar preparation, mulberry rods are used as the raw material. Because the surfaces of most of the biochar are predominantly net negatively charged [13], their sorption efficiency to aqueous phosphorus which is in anionic forms, is relatively low [14]. Several methods have thus been developed to modify biochar to enhance its sorption of phosphorus. Biochar modified with iron oxide magnetic showed a strong ability to remove phosphorus from aqueous solution [15].

Iron manganese oxide modified mulberry biochar (IMOM-BC) was prepared by the combined modification of mulberry biochar (M-BC) with potassium permanganate, ferrous chloride, triethylenetetramine, and epichlorohydrin. Scanning electron microscope (SEM), Fourier-transform infrared spectroscopy (FTIR), X-ray diffraction (XRD), and X-ray photoelectron spectroscopy (XPS) were used to characterize the structural differences between the M-BC and the IMOM-BC. The sorption of phosphorus by the IMOM-BC and the companion M-BC were compared, and the adsorption mechanism of IMOM-BC for phosphorus was carefully analyzed.

2. Materials and methods

2.1. Reagents

The employed potassium dihydrogen phosphate and concentrated sulfuric acid are Guaranteed reagent; potassium permanganate, ferrous chloride, triethylenetetramine, epichlorohydrin, ascorbic acid, ammonium molybdate, and bismuth potassium tartrate are analytical grade. All reagents were purchased from Shanghai Guoyao Group Chemical Reagent Co. Ltd., China. All solutions were prepared by ultrapure water.

2.2. Analytical instruments

The following analytical instruments were utilized in the analysis of samples. NICOLET 6700 Fourier infrared spectrum analyzer (Japan Hitachi Company, Japan); X'Pert PROX diffractometer (PANalytical, Netherlands); SDTQ600 synchronous thermogravimetric analyzer (TA company, USA); JSM-7900F SEM (JEOL, Japan); NOVA 2000e automatic surface ratio analyzer (Quantachrome, USA).

2.3. Preparation of IMOM-BC

The peeled and broken Mulberry rods were placed in a muffle furnace and calcined at 500°C for 3 h, and passed through a 100 mesh sieve to get M-BC. Three grams of M-BC was placed in a 200 mL beaker, and 100 mL of a mixed solution of 0.1 mol/L of ferrous chloride and 0.025 mol/L of magnesium chloride was added and stirred for 10 min. After immersion for 3 h, 1 mL of polyethylene glycol (PEG), 100 mL of potassium permanganate solution with a concentration of 0.05 mol/L, 20 mL of 10% sodium hydroxide solution, and 10 mL of epichlorohydrin were added to the beaker in turn, and were heated at 60°C for 3 h. Then, 5 mL of triethylenetetramine was added, and the reaction was carried out at 80°C for 6 h. The obtained IMOM-BC was then cooled and filtered and passed through 100 mesh for use [16].

2.4. Batch experiments

Phosphorus-containing simulated solutions with different concentrations were prepared by dissolving potassium dihydrogen phosphate in ultrapure water, and the pH values of phosphate solutions was adjusted to a required pH value with diluted NaOH (0.1 mol/L) or HCl (0.1 mol/L), 0.1 g of adsorbent was added to 100 mL polyethylene plastic centrifuge tube, and 50 mL phosphorus-containing simulated solution adjusted to the required pH was then added to the tube. After the centrifuge tube was oscillated at 200 r/min in a constant temperature water bath oscillator for a set time, the centrifuge tube was removed, and the supernatant was filtered through a 0.45 mm filter. The aqueous phosphorus concentration was determined by the Mo-Sb molybdenum blue spectrophotometry method.

3. Results and discussion

3.1. Characterization of biochar and IMOM-BC

3.1.1. BET surface area

The BET surface area and pore volume of the M-BC were 175.391 m^2/g and 0.143 cm^3/g, respectively, which were larger than the BET surface area and pore volume of the IMOM-BC were 74.734 m^2/g and 0.094 cm^3/g, respectively. The pore diameter of M-BC was 3.259 nm, whereas the pore diameter of IMOM-BC was 5.042 nm, and the pore diameter of IMOM-BC was 35.4% higher than that of M-BC. This may be the reason for the decrease in the specific surface area and pore volume after modification [17]. It is indicated that the pore diameter of M-BC can be improved by modification, which is beneficial to the entry of macromolecular phosphorus into the pores of biochar.

3.1.2. Zeta potential

The zeta potential of IMOM-BC (Fig. 1) illustrates that the point of zero charge value (pH_{zpc}) of IMOM-BC is 7.6. When the pH is less than 7.6, the surface of the adsorbent is protonated, and the surface of IMOM-BC is positively charged, which is beneficial for electrostatic attraction between the surface groups and phosphorus species might occur. When the pH is greater than 7.6, the surface of IMOM-BC is

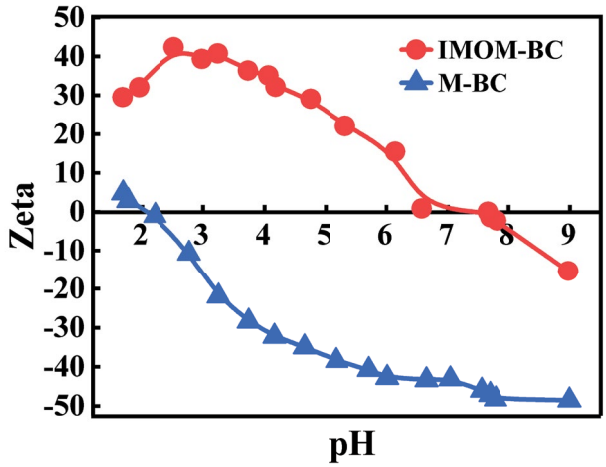

Fig. 1. Zeta potential of IMOM-BC and M-BC.

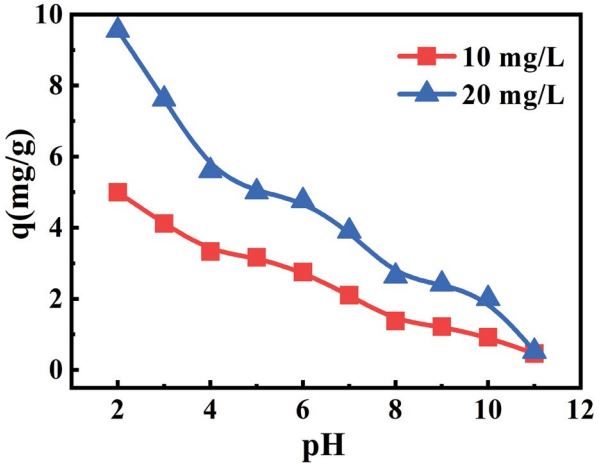

Fig. 2. Effect of pH on the phosphorus by IMOM-BC.

negatively charged, and the adsorption effect for total phosphorus becomes poor. Compared with IMOM-BC, the pH_{zpc} of M-BC is 2.19. After modification, the loading of metal oxides is beneficial to increase the positive charge on the surface of the biochar, and increase its pH_{zpc}, which is beneficial to the adsorption of phosphorus.

3.2. Major factors affecting the adsorption of phosphorus

3.2.1. Effect of initial pH on the adsorption of phosphorus

The pH value of the solution is usually considered to be an essential factor in affecting the adsorption of ions [18]. As shown in Fig. 2, the adsorption amount of phosphorus gradually decreases with an increase in pH value. When pH is 2.0, the adsorption capacity is the largest, which is consistent with the findings of Liu [19] and Zong [20]. This phenomenon is related to the mechanism of adsorption of phosphorus by IMOM-BC, which includes ion exchange, van der Waals force, and acid-base reaction. Due to the differences in the pH values of the solution, the form of phosphorus also changes. Significant differences in the adsorption effects that were dependent on the pH range were noted, which could be attributed to the form of phosphorus. At pH < 2.2, phosphate in water is mainly in the form of H_3PO_4; at 2.2 < pH < 7.2, $H_2PO_4^-$; at 7.2 < pH < 9.0, HPO_4^{2-}; and at pH > 9.0, PO_4^{3-}. When pH is lower than the zero point of charge (pH_{zpc} = 7.6) of the IMOM-BC, the surface of the IMOM-BC is protonated and becomes positively charged. Under this condition, the phosphate is adsorbed on the surface of IMOM-BC under electrostatic attraction and ion exchange. When pH is higher than the pH_{zpc} of the IMOM-BC, causing a large amount of OH^- to accumulate on the surface of the adsorbent and is negatively charged, therefore the aqueous phosphorus concentration increases with a gradual increase in the pH. Phosphate is present as an anion form (phosphate ion) in the solution, which produces electrostatic repulsion and leads to a decrease in the amount of phosphorus adsorption capacity. At the same time, the concentration of OH^- in the solution occupies a part of the active adsorption sites on the surface of the adsorbent, which competes with the phosphate in the adsorption. It further reduces the adsorption of phosphorus on the adsorbent [21].

3.2.2. Effect of contact time on the adsorption of phosphorus

As shown in Fig. 3, the amount of phosphorus adsorbed by IMOM-BC gradually increases during the adsorption experiment in the first 10 h, then it tends to be stable. Which was typical of ion adsorption from dilute aqueous solutions and indicative of favor interactions between IMOM-BC and phosphorus. Results in Fig. 3 also show that the amount of phosphorus adsorption reached a saturation at 12 and 20 h at the initial phosphorus concentration of 10 and 20 mg/L, respectively, under experimental condition of 25°C and pH 2.0. It was observed further that phosphorus was adsorbed within the first 5 h at an average adsorption rate of 0.0133 mg/g per minute when the initial phosphorus concentration was 10 mg/L, temperature at 25°C and pH 2.0. A similar trend for initial phosphorus concentration of 20 mg/L was also observed. There were reports that adsorption reaction occurred rapidly during the initial stage, which was followed by a slow reaction till equilibrium [22]. The presence of a large number of vacant sites at the initial stage may be the cause of initial uptake of adsorbate species [23].

3.2.3. Effect of dosage on the adsorption of phosphorus

The effect of dosage (Fig. 4) indicates that the removal rate of phosphorus tends to increase significantly with the increase of IMOM-BC dosage, but the unit adsorption amount of phosphorus by IMOM-BC gradually decreased. When the dosage of IMOM-BC was 0.4 g/L, the removal rates of IMOM-BC for the initial concentration of 10 and 20 mg/L of phosphorus solution were 37.13% and 25.31%, respectively. When the dosage of IMOM-BC was increased to 2.0 g/L, the removal rate of phosphorus by IMOM-BC increased to 99.85% and 95.23%, respectively.

As the dosage continued to increase, the rate of removal of phosphorus is increased mildly, and the unit adsorption amount is reduced significantly. The main reason could be

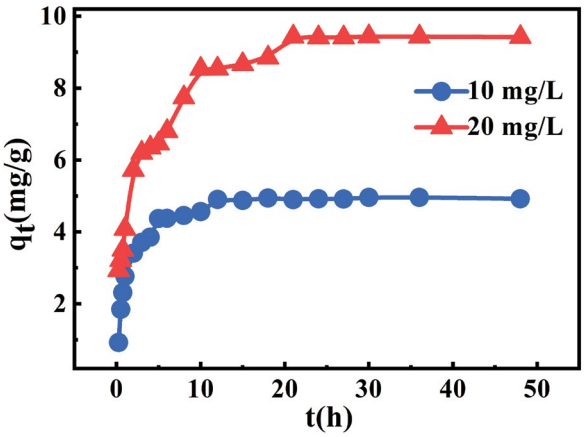

Fig. 3. Effect of contact time on the adsorption of phosphorus by IMOM-BC.

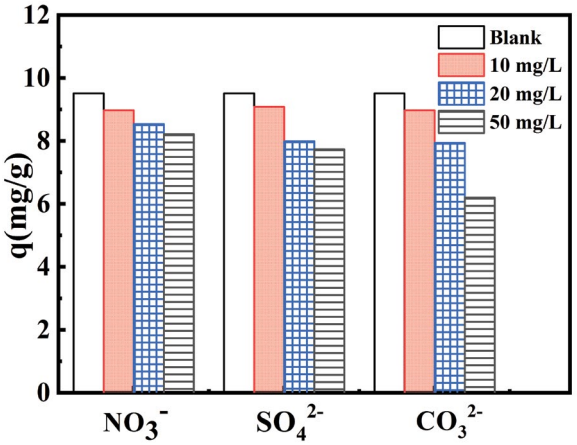

Fig. 5. Effect of coexisting anions on the adsorption of phosphorus by IMOM-BC.

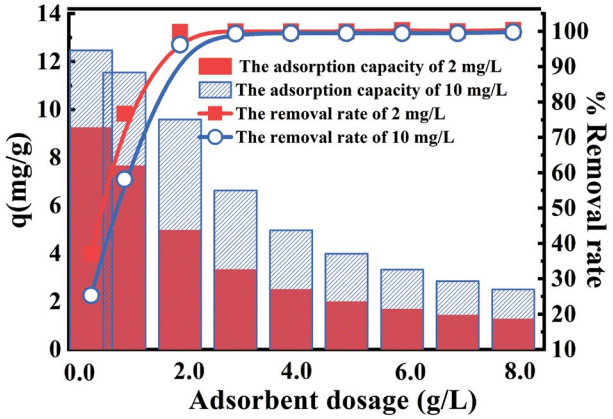

Fig. 4. Effect of dosage on the adsorption of phosphorus by IMOM-BC.

that the adsorption rate is increased with the increase of dosage, leading to an increase in the removal rate. But the adsorption per unit amount of the adsorbent is decreased. Considering the removal effect and the adsorption amount of the adsorbent, 2.0 g/L adsorbent was selected as the optimum dosage.

3.2.4. Coexisting anions

A large number of inorganic anions exist in the solution, for example, NO_3^-, CO_3^{2-}, SO_4^{2-}, etc. They compete with phosphorus for adsorption, which reduces the adsorption capacity of the adsorbent for phosphorus. Different concentrations of NO_3^-, CO_3^{2-}, and SO_4^{2-} have different effects on the removal of phosphorus (Fig. 5). The order of inhibition in the adsorption process is: $CO_3^{2-} > SO_4^{2-} > NO_3^-$, wherein the negative effect of CO_3^{2-} on the removal of phosphorus by the IMOM-BC is relatively large, and the adsorption amount of phosphate is reduced from 9.44 to 6.20 mg/g, which may be attributed to the hydrolysis of carbonate in aqueous solution, resulting in an increase in the amount of anions in the solution. Phosphate and other anions can form endosphere complexes with metal oxides [8], so that coexisting anions and phosphate ions can compete to the active adsorption sites for adsorption. Different anions have different degrees of inhibition on the adsorption of phosphorus, which may be caused by the differences in the affinity between the anions and IMOM-BC [24,25].

3.3. Adsorption isotherm

The adsorption isotherm of phosphorus by IMOM-BC was shown in Fig. 6. It can be seen from Fig. 6 that the adsorption amount of phosphate by IMOM-BC is significantly improved as compared to the adsorption amount of phosphate by M-BC, which increased from 5.02 to 23.09 mg/g. As the temperature increased from 25°C to 45°C, the amount of adsorption of phosphate increased from 23.09 to 26.34 mg/g, indicating that the amount of adsorption was positively correlated with temperature. IMOM-BC exhibited a phosphorus adsorption capacity of 23.26 mg/g, which was higher than 9.62 mg/g of nano-zero-valent iron modified pomelo peel biochar [26] and 12.86 mg/g of KOH modified activated sludge biochar [27], slightly higher than 15.46 mg/g of $ZnCl_2$ modified sesame straw biochar [28] and 17.04 mg/g of magnesium-supported taro straw biochar [29]. However, the phosphorus adsorption density of IMOM-BC was much greater than 5.02 mg/g of M-BC at 25°C.

The Langmuir and Freundlich adsorption model equations were cited to fit the experimental data of IMOM-BC for phosphorus and to obtain adsorption isotherms, as shown in Eqs. (1) and (2), respectively. And results for their fitting curves were plotted (Fig. 7).

Langmuir:

$$\frac{C_e}{q_e} = \frac{1}{K_L q_{\max}} + \frac{C_e}{q_{\max}} \quad (1)$$

where $q_{\max}$ is the maximum adsorption capacity of the adsorbent (mg/g) and K_L (L/mg) is the Langmuir constant, which is related to the energy of adsorption, the values of q_e, K_L, and R^2 are presented in Table 1.

Freundlich:

$$\ln q_e = \ln K_F + \frac{1}{n}\ln C_e \quad (2)$$

where K_F (L/g) is the Freundlich constant related to the adsorption capacity of the adsorbent and $1/n$ is a constant related to the adsorption intensity, the values of K_F, $1/n$, and R^2 are presented in Table 1.

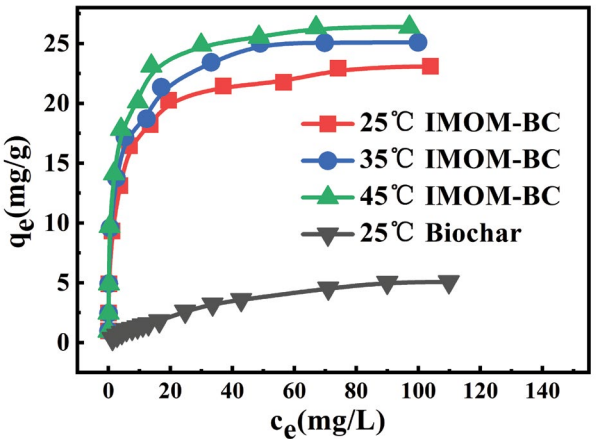

Fig. 6. Adsorption isotherms of phosphorus with IMOM-BC.

From Table 1, the correlation coefficients (R^2) of the Langmuir model equation fitting at 25°C, 35°C, and 45°C are 0.999, 0.998, and 0.999, respectively, which confirms the existence of a better correlation. The maximum adsorption capacity of phosphorus at 25°C, 35°C, and 45°C are 23.09, 25.32, and 26.34 mg/g, respectively. Langmuir model best describes the adsorption process, which shows monolayer adsorption of phosphorus by IMOM-BC [18]. Lai et al. [30] reported a similar conclusion by treating phosphorus-containing wastewater with magnetic Fe-Zr oxide. Zhang et al. [31] used bentonite as a raw material to adsorb phosphorus in wastewater by hydrazine modification, and a similar outcome was noted. At 25°C, 35°C, and 45°C, R^2 fitting by Freundlich equation are 0.863, 0.848, and 0.819, respectively, which indicates a weak correlation. This adsorption process cannot be accurately represented. By comparing the two fitting equations, IMOM-BC is more in line with the Langmuir equation for the removal of phosphorus. It was observed further that increasing the temperature is beneficial to increase the removal of phosphorus. This may be attributed to that an increase in temperature reduces the viscous forces in the solution. This accelerates the rate of diffusion of ions, and may also increase the degree of activation of the adsorbent, which is beneficial to the progress of the chemical adsorption [32].

3.4. Dynamic adsorption

The effect of influent phosphorus concentration on the breakthrough curves (Fig. 8) illustrated that the adsorption

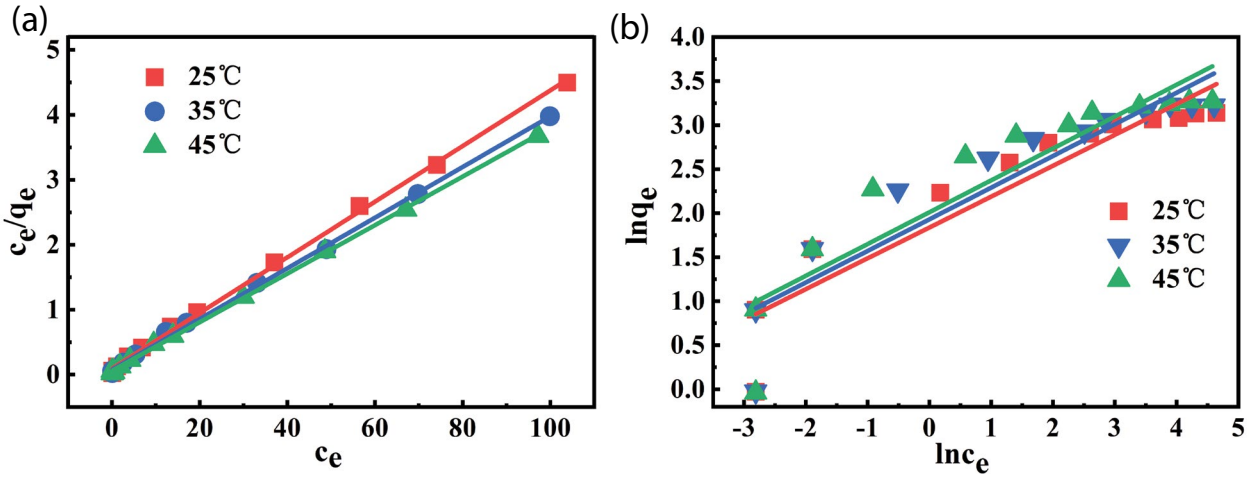

Fig. 7. Isotherm fit (a) Langmuir Isotherm and (b) Freundlich Isotherm.

Table 1
Adsorption isotherm parameters at different temperatures

Temperature (°C)	$q_{e,exp}$ (mg/g)	Langmuir			Freundlich		
		R^2	K_L	q_e (mg/g)	R^2	K_F	$1/n$
25	23.09	0.999	1.105	23.26	0.863	17.473	0.357
35	25.32	0.998	1.213	25.41	0.848	19.043	0.359
45	26.34	0.999	1.226	26.39	0.819	26.102	0.362

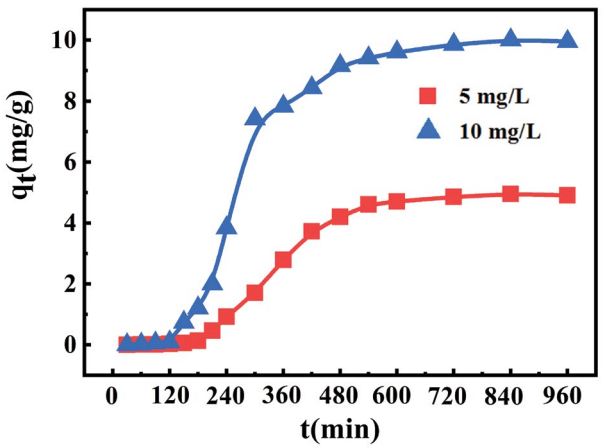

Fig. 8. Effect of influent phosphorus concentration on the breakthrough curve of phosphorus adsorption on IMOM-BC. Conditions: bed depth 1.0 cm; flow rate 5.0 mL/min; pH = 2.0.

process reached saturation faster and the breakthrough time decreased with increasing influent phosphorus concentration. A decrease in phosphorus concentration gave a later breakthrough curve, and the treatment time was the greatest at the lowest influent concentration. As the initial concentration of phosphorus increases, the driving force for adsorption (C_0–C_e), and hence the rate of adsorption increases, so that the time for adsorption to reach saturation is relatively shortened. With progress in the adsorption time, the adsorption zone in the adsorption column also moves. When the adsorption zone moves to the end of the adsorption column, the effluent concentration increases sharply. To further analyze its dynamic adsorption behavior, the dynamic adsorption was fitted using the Thomas and Yoon–Nelson models, which have been expressed in Eqs. (3) and (4), and their fitting curves are shown in Fig. 9.

Thomas model:

$$\ln\left(\frac{C_0}{C_t}-1\right)=\frac{K_{TH}q_t m}{Q}-K_{TH}C_0 \tag{3}$$

where q_t is the amount of total phosphorus adsorbed per gram of IMOM-BC (mg/g). The values of K_{TH} (Thomas rate constant) and q_t were determined by plotting C_t/C_0 against t using linear regression analysis [33].

Yoon-Nelson model:

$$\ln\left(\frac{C_t}{C_0-C_t}\right)=K_{YN}t-K_{YN}t_{\frac{1}{2}} \tag{4}$$

where K_{YN} is the Yoon–Nelson rate constant; $t_{1/2}$ is the time required for 50% adsorbate breakthrough (min), and t is the breakthrough time (min). The parameters K_{YN} and $t_{1/2}$ are determined by plotting $\ln[C_t/(C_0–C_t)]$ vs. time (min) [34].

It can be noted from Fig. 9 that when the initial concentration is 5 mg/L, the total concentration of phosphorus in the effluent within 200 min of the initial stage of adsorption is close to zero. After 540 min of adsorption, the total concentration of phosphorus in the effluent gradually increased to 92.2% of the influent concentration. When the initial concentration of the solution was 10 mg/L, the total concentration of phosphorus increased to 91.6% of the influent concentration after 420 min. It indicates that as the initial total phosphorus concentration increases, the driving force (C_0–C_e) for the adsorption increases gradually, and the rate of adsorption increases so that the time to reach saturation is relatively shortened. At 5 and 10 mg/L, R^2 fitting by Thomas was 0.934 and 0.927, respectively; R^2 of the Yoon–Nelson fitting at 5 and 10 mg/L was 0.937 and 0.944, respectively; Yoon–Nelson fitting is closer to 1 than that fitting by Thomas, which is more suitable for describing the dynamic adsorption process of phosphorus by IMOM-BC.

3.5. Stability of adsorbent

The concentrations of iron and manganese in the adsorption equilibrium of IMOM-BC for the adsorption of phosphorus-containing water (phosphorus concentration of 20.0 mg/L) were determined under different initial pH values. At the initial pH of 2.0–11.0 (balanced pH of 2.1–10.4), manganese ions were not detected in the solution. It indicates that manganese in the adsorbent was present in

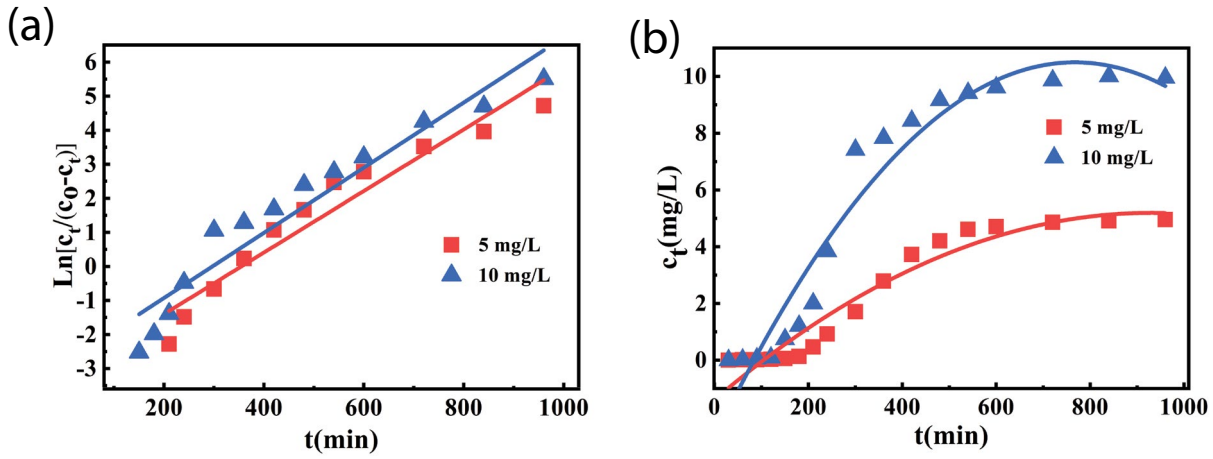

Fig. 9. Linear fitting (a) Thomas model and (b) Yoon–Nelson model.

a relatively stable form. At an initial pH of 2.0 (balanced pH of 2.1), the concentration of iron in the solution was 0.056 mg/L. When the pH > 2, iron was not detected in the solution, which shows that the adsorbent has excellent stability under the experimental pH conditions.

4. Chemical interaction of phosphorus with IMOM-BC

4.1. Scanning electron microscopy

SEM/EDS (energy dispersive spectroscopy) analysis results of IMOM-BC and M-BC (Fig. 10) show different pores structure, IMOM-BC has more and better pore structures than M-BC. It may be attributed to that after IMOM-BC was calcined at 500°C, the oxidized and modified pores of the M-BC did not collapse or was not broken. Fe, Mn, and Mg are found being oxidized into granular oxides and then attached to the surface of the pores of the M-BC (Fig. 10a). This proves the success in the modification of M-BC. It can be observed further that P peak presents in pattern of IMOM-BC after phosphorus adsorption (Fig. 10b), confirming phosphorus adsorption on IMOM-BC.

4.2. X-ray diffraction

The X-ray diffraction pattern of IMOM-BC before and after phosphorus adsorption were measured (Fig. 11). It shows that the natural charcoal does not have any apparent crystal structure before phosphorus adsorption, and IMOM-BC exhibits an amorphous structure. The X-ray diffraction analysis showed an obvious structural change in the IMOM-BC after phosphorus adsorption. The diffraction peaks of MnP (Reference code 00-007-0384) and FeP_4 (Reference code 00-034-0995) were recognized after phosphorus adsorption. It indicates that phosphorus may react with iron and manganese on the surface of IMOM-BC during the adsorption process.

4.3. Fourier-transform infrared spectroscopy

FTIR spectra results of M-BC and IMOM-BC (Fig. 12) indicate that FTIR adsorption peak position of M-BC was unchanged, but modifies lightly the intensity of FTIR adsorption peaks. Strong and broad bands at 3,400 cm^{-1} indicates that IMOM-BC contains a large number of hydroxyl groups. The absorption peak at 1,619 cm^{-1} is attributed to the stretching vibrations of –C=C and –C=O [35]. After adsorption of phosphorus by IMOM-BC, two new adsorption peaks appear at around 1,058 and 1,385 cm^{-1}, the absorption peak at 1,058 cm^{-1} is the characteristic absorption

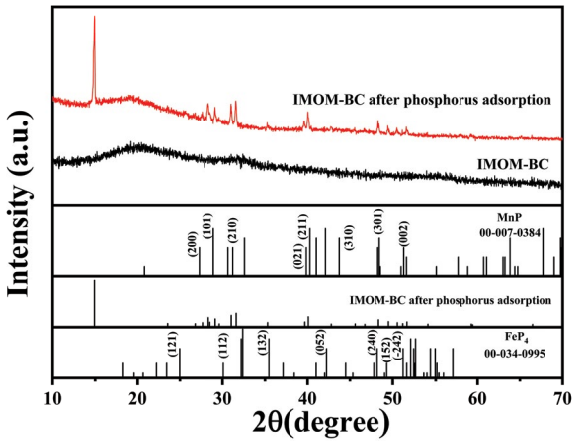

Fig. 11. XRD spectrum of IMOM-BC before and after adsorption of phosphorus.

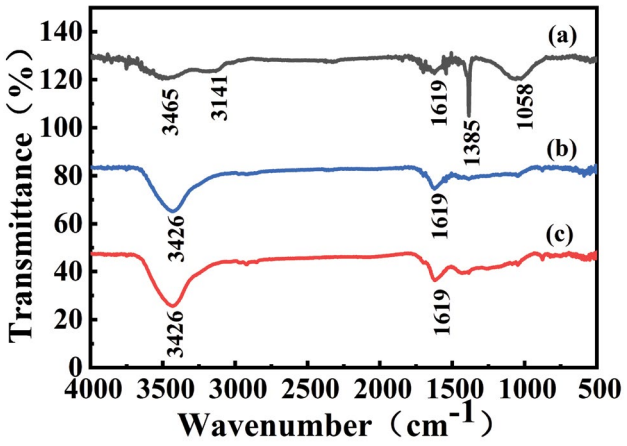

Fig. 12. FTIR spectra of IMOM-BC and M-BC. (a) IMOM-BC after adsorption, (b) IMOM-BC, and (c) M-BC.

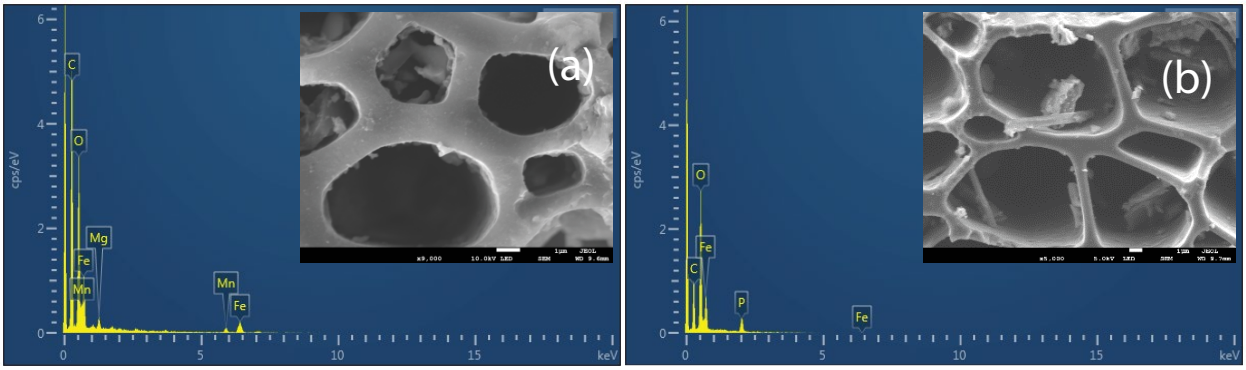

Fig. 10. SEM/EDS micrograph of IMOM-BC and M-BC. (a) M-BC and (b) IMOM-BC.

peak of P–O vibration. The above indicates the formation of an inner spherical surface complex between phosphate and metal oxide [36]. It could be noted that the absorption peak at 3,400 cm^{-1} attenuates, indicating that the surface hydroxyl and phenolic hydroxyl groups of the adsorbent participate in the adsorption. Therefore, the surface hydroxyl group (M–OH) of the adsorbent might exchange with the phosphate. Combined with the FTIR spectra, the functional groups on the surface of the adsorbent confirm its adsorption characteristics and proves the improvements in its adsorption capacity [37,38].

4.4. X-ray photoelectron spectroscopy

The results of Full-scan XPS spectra of the IMOM-BC and the IMOM-BC after phosphorus adsorption are shown in Fig. 13. The corresponding orbital binding energy data are listed in Table 2. The observed photoelectron signals were carbon C1s (284.01–284.05 eV), O1s (530.56–530.81 eV), Fe2p (710.01–710.48 eV), and Mn2p (125,640.33–640.59 eV) were presented in Fig. 13a and b, since phosphor constitutes only 2.32% (Table 2) of the IMOM-BC after phosphorus adsorption chemical composition and its XPS sensitivity factor is relatively low. The positional binding energy of iron and

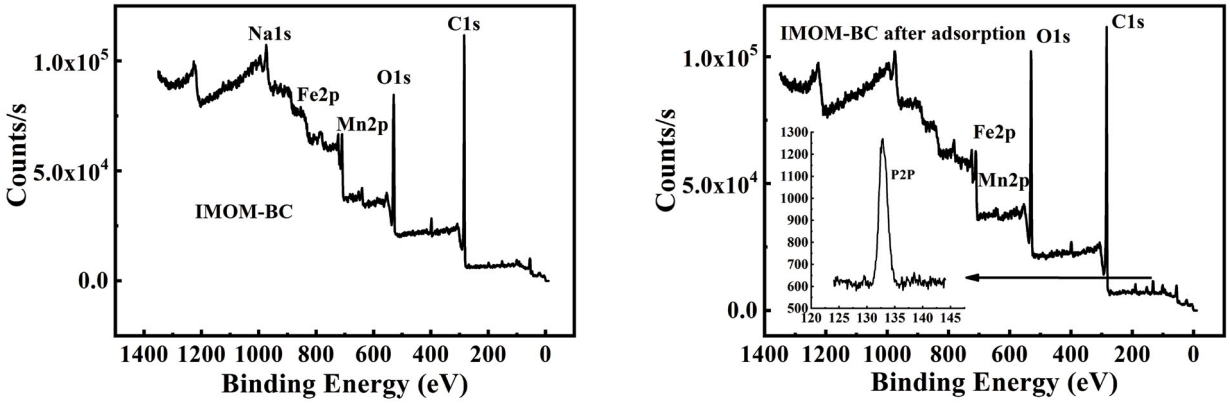

Fig. 13. Full-scan XPS spectra of IMOM-BC before and after phosphorus adsorption.

Table 2
Binding energy (eV) and composition (%) of the most intense photoelectron peaks of IMOM-BC before and after adsorption phosphorus as determined by XPS

	Binding energy (eV)					Composition (%)				
Sample	C1s	O1s	Fe2p	Mn2p	P2p	C1s	O1s	Fe2p	Mn2p	P2p
IMOM-BC	284.05	530.56	710.01	640.33	–	71.68	23.07	4.24	1.00	–
IMOM-BC After phosphorus adsorption	284.01	530.81	710.48	640.59	132.87	67.77	25.43	3.51	0.52	2.32

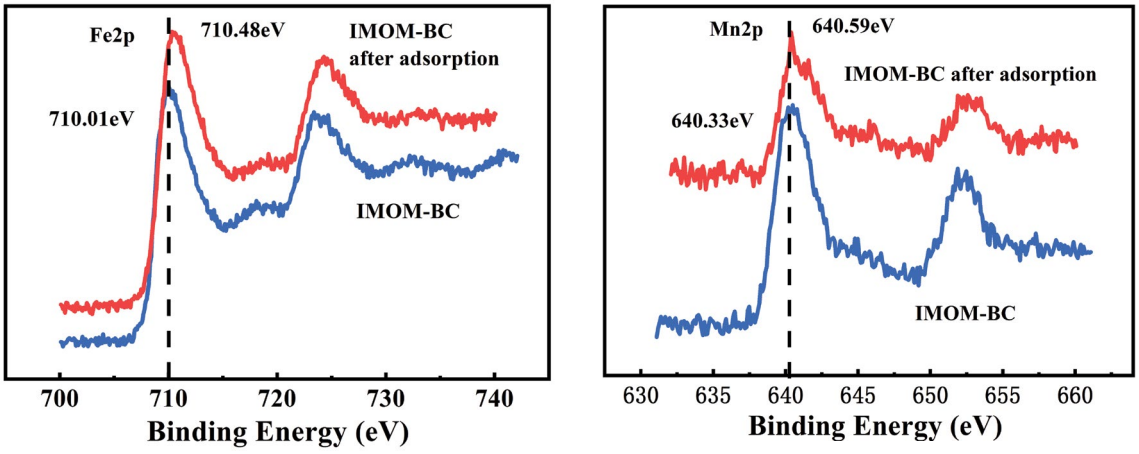

Fig. 14. XPS spectra of Fe and Mn before and after phosphorus adsorption.

manganese atoms of the IMOM-BC and the IMOM-BC after phosphorus adsorption are shown in Fig. 14. It could be seen that the binding energy of Fe2p of IMOM-BC shift from 710.01 to 710.48 eV after phosphorus adsorption. The binding energy of Mn2p of IMOM-BC shifts from 640.33 to 640.59 eV, which indicates that iron and manganese oxides in the IMOM-BC involved in the adsorption process. The peak center at 132.87 eV (Fig. 13a) is attributed to the P2p. This further indicates that phosphorus is chemisorbed on the surface of the IMOM-BC. This is consistent with the results obtained from FTIR analysis.

5. Conclusion

IMOM-BC was mainly composed of Fe, Mn oxides, and has a microporous structure with a specific surface area of 74.734 m^2/g and the pH_{zpc} values of the IMOM-BC was 7.6. Major oxygen-containing functional groups and hydroxyl groups were present abundantly on the surfaces of IMOM-BC. The optimum phosphorus adsorption occurred in the pH 2.0. Different anions have different effects on the removal of phosphorus by IMOM-BC, and the order of inhibition is: $CO_3^{2-} > SO_4^{2-} > NO_3^-$. At 25°C, 35°C, and 45°C, the maximum adsorption capacities of phosphorus were 23.09, 25.32, and 26.34 mg/g, respectively. The iron oxide, manganese oxide, surface hydroxyl group, and phenolic hydroxyl group in IMOM-BC participate in the adsorption. The adsorption of phosphorus by IMOM-BC is mainly attributed to a chemical reaction, and the IMOM-BC has good stability during adsorption.

Acknowledgments

This paper has greatly benefited from the insightful comments of anonymous reviewers. This research was financially assisted by Guangxi Natural Science Foundation Project (2017GXNSFAA198186) and the National Natural Science Foundation of China (NSFC21367010), and supported by Guangxi science and Technology Planning Project under Grant (No. GuiKe-AD18126018).

References

[1] Q.Q. Yin, B.D. Zhang, R.K. Wang, Z.H. Zhao, Biochar as an adsorbent for inorganic nitrogen and phosphorus removal from water: a review, Environ. Sci. Pollut. Res., 24 (2017) 26297–26309.
[2] L.Z. Song, J.B. Huo, X.L. Wang, F.F. Yang, J. He, C.Y. Li, Phosphate adsorption by a Cu(II)-loaded polyethersulfone-type metal affinity membrane with the presence of coexistent ions, Chem. Eng. J., 284 (2016) 182–193.
[3] D. Franco, J. Lee, S. Arbelaez, N. Cohen, J-Y. Kim, Removal of phosphate from surface and wastewater via electrocoagulation, Ecol. Eng., 108 (2017) 589–596.
[4] X.X. Zhou, Adsorption Behavior and Mechanism of Arsenic on Mesoporous Silica Modified by Iron-Manganese Binary Oxide ($FeMnO_x$/SBA-15) from Aqueous Systems, Zhejiang University, Zhejiang, China 2018.
[5] H.L. Liu, M.N. Liang, Y. Zhu, F.F. Cai, H.X. Zou, The adsorption of arsenic by ferric hydroxide and its precipitation mechanism, Acta Sci. Circumstantiae, 29 (2009) 1011–1020.
[6] J. Tong, Z.H. Yang, G.M. Zeng, W.P. Xiong, J. Huang, H.Y. Xu, P.P. Song, Preparation of hydroxyl-iron-zirconium modified activated carbon fieber and its phosphate removal performance, Chin. J. Environ. Eng., 10 (2016) 2881–2888.
[7] S.B. Kanungo, S.S. Tripathy, S.K. Mishra, B. Sahoo, Rajeev, Adsorption of Co^{2+}, Ni^{2+}, Cu^{2+}, and Zn^{2+} onto amorphous hydrous manganese dioxide from simple (1–1) electrolyte solutions, J. Colloid Interface Sci., 269 (2004) 11–21.
[8] R. Han, W. Zou, H. Li, Y. Li, J. Shi, Copper(II) and lead(II) removal from aqueous solution in fixed-bed columns by manganese oxide coated zeolite, J. Hazard. Mater., 137 (2006) 934–942.
[9] M.L. Jiang, H. Jin, C. Deng, S. Wang, Preparation and characterization of nanoparticles containing Fe_3O_4 cores in biochar, J. Agro Environ. Sci., 37 (2018) 592–597.
[10] K. Namratha, K. Byrappa, Hydrothermal processing and in situ surface modification of metal oxide nanomaterials, J. Supercrit. Fluids.,79 (2013) 251–260.
[11] X.P. Zheng, Characteristic Adsorption of Nitrate and Hexavalent Chromium in Aqueous Solution by Iron and Manganese Oxide/Biochar Composites, Northwest University, China, 2013.
[12] Statistical Communique of National Economic and Social Development of Guangxi Zhuang Autonomous Region, 2016. Available at: http://www.gxtj.gov.cn/tjsj/tjgb/qqgb/201704/t20170417_132996.html
[13] Y. Yao, B. Gao, M. Zhang, M. Inyang, A.R. Zimmerman, Effect of biochar amendment on sorption and leaching of nitrate, ammonium, and phosphate in a sandy soil, Chemosphere, 89 (2012) 1467–1471.
[14] L. Beesley, M. Marmiroli, The immobilisation and retention of soluble arsenic, cadmium and zinc by biochar, Environ. Pollut., 159 (2011) 474–480.
[15] B.L. Chen, Z.M. Chen, S.F. Lv, A novel magnetic biochar efficiently sorbs organic pollutants and phosphate, Bioresour. Technol., 102 (2011) 716–723.
[16] M.N. Liang, X. Cheng, D.Q. Wang, S.P. Xu, L.L. Yan, Z.Q. Zhu, Preparation Method of Modified Mulberry Tree Biomass Carbon Adsorbent, National Intellectual Property Administration, PRC, China, 2018.
[17] Q. Chang, G.D. Jiang, M.X. Hu, J. Huang, H-Q. Tang, Adsorption of Methylene Blue from aqueous solution onto magnetic Fe_3O_4/graphene oxide nanoparticles, J. Environ. Sci., 35 (2014) 1804–1809.
[18] K. Komnitsas, D. Zaharaki, G. Bartzas, G. Alevizos, Adsorption of scandium and neodymium on biochar derived after low-temperature pyrolysis of sawdust, Minerals, 7 (2017) 200.
[19] K. Liu, Efficiency and Mechanism of Phosphorus Removal by Combined Use $KMnO_4$ and $FeSO_4$, Harbin Institute of Technology, China, 2010.
[20] E.M. Zong, A Adsorptive Removal of Phosphate Ions from Aqueous solution using Zirconia-Functionalized Carbonaceous Materials, Nanjing University, China, 2013.
[21] F.H. Li, W.H. Wu, R.Y. Li, X.R. Fu, Adsorption of phosphate by acid-modified fly ash and palygorskite in aqueous solution: experimental and modeling, Appl. Clay Sci., 132 (2016) 343–352.
[22] P.C. Brandao, T.C. Souza, C.A. Ferreira, C.E. Hori, L.L. Romanielo, Removal of petroleum hydrocarbons from aqueous solution using sugarcane bagasse as adsorbent, J. Hazard. Mater., 175 (2010) 1106–1112.
[23] D. Kavitha, C. Namasivayam, Experimental and kinetic studies on methylene blue adsorption by coir pith carbon, Bioresour. Technol., 98 (2007) 14–21.
[24] F. Yang, S. Zhang, Y. Sun, D.C.W. Tsang, K. Cheng, Y.S. Ok, Assembling biochar with various layered double hydroxides for enhancement of phosphorus recovery, J. Hazard. Mater., 365 (2019) 665–673.
[25] Z.L. Shi, F.M. Liu, S.H. Yao, Adsorptive removal of phosphate from aqueous solutions using activated carbon loaded with Fe(III) oxide, New Carbon Mater., 26 (2011) 299–306.
[26] B. Chen, J.J. Lian, S.S. Wang, B. Dai, T.N. Ye, Preparation of modified pomelo peel biochars and its phosphate removal in aqueous solution, J. Anhui. Univ. Technol. Sci., 35 (2018) 125–130.
[27] A. Spataru, R. Jain, J.W. Chung, G. Gerner, R. Krebs, P.N.L. Lens, Enhanced adsorption of orthophosphate and copper onto hydrochar derived from sewage sludge by KOH activation, RSC Adv., 21 (2019) 11595–11601.

[28] J.H. Park, Y.S. Ok, S.H. Kim, J.S. Cho, J.S. Heo, R.D. Delaune, D.C. Seo, Evaluation of phosphorus adsorption capacity of sesame straw biochar on aqueous solution: influence of activation methods and pyrolysis temperatures, Environ. Geochem. Health, 37 (2015) 969–983.
[29] Y.H. Jiang, A.Y. Li, H. Deng, C.H. Ye, Y.Q. Wu, Y.D. Linmu, H.L. Hang, Characteristics of nitrogen and phosphorus adsorption by Mg-loaded biochar from different feedstocks, Bioresour. Technol., 276 (2019) 183–189.
[30] L. Lai, Q. Xie, L. Chi, W. Gu, D.Y. Wu, Adsorption of phosphate from water by easily separable Fe_3O_4@SiO_2 core/shell magnetic nanoparticles functionalized with hydrous lanthanum oxide, J. Colloid Interface Sci., 465 (2016) 76–82.
[31] J.D. Zhang, Z.M. Shen, W.P. Shan, Z.Y. Chen, Z.J. Mei, Y.M. Lei, W.H. Wang, Adsorption behavior of phosphate on lanthanum(III) doped mesoporous silicates material, J. Environ. Sci., 22 (2010) 507–511.
[32] M.F. Torres, J.M. González, M.R. Rojas, A.J. Müller, A.E. Saez, D. Lof, K. Schillén, Effect of ionic strength on the rheological behavior of aqueous cetyltrimethylammonium p-toluene sulfonate solutions, J. Colloid Interface Sci., 307 (2007) 221–228.
[33] H.N. Lan, M.V. Thi, T.L. Thi, T.T. Van, P.T. Thi, T.V. Huu, Ammonium removal from aqueous solutions by fixed-bed column using corncob-based modified biochar, Environ. Technol., 40 (2019) 683–692.
[34] S.H. Hasan, D. Ranjan, M. Talat, Agro-industrial waste 'wheat bran' for the biosorptive remediation of selenium through continuous up-flow fixed-bed column, J. Hazard. Mater., 181 (2010) 1134–1142.
[35] X.T. Jiang, J. Chi, Phosphorus adsorption by and forms in Fe-modified biochar, J. Agro Environ. Sci., 33 (2014) 1817–1822.
[36] S.Y. Yoon, C.G. Lee, J.A. Park, J.H. Kim, S.B. Kim, S.H. Lee, J.W. Choi, Kinetic equilibrium and thermodynamic studies for phosphate adsorption to magnetic iron oxide nanoparticles, Chem. Eng. J., 236 (2014) 341–347.
[37] Y.M. Qin, D.Q. Wang, M.N. Liang, Preparation of mulberry stem activated carbon/Fe-Mn oxide composite sorbent and its effects on the adsorption of Cr(VI), Environ. Chem., 35 (2016) 783–792.
[38] W.Y. Huang, J. Chen, F. He, J.P. Tang, D. Li, Y. Zhu, Y.M. Zhang, Effective phosphate adsorption by Zr/AL-pillared montmorillonite: insight into equilibrium, kinetics and thermodynamics, Appl. Clay Sci., 104 (2015) 252–260.